The Evolution and Present State of Tree-Kills on Mammoth Mountain, California: Tracking Volcanogenic CO_2 and Its Lethal Effects

Brigette A. Martini and Eli A. Silver[1]

1.0 INTRODUCTION

In May 1989, a small magnitude earthquake swarm hit the east-central region of the Sierra Nevada in the state of California. The swarm was located beneath the Pleistocene-aged Mammoth Mountain - a rhyodacitic stratovolcano located on the southwestern rim of the much larger, 760,000 year-old Long Valley caldera (see Figure 1). Early earthquakes of the swarm were probably due to magmatic dike intrusion at depth (Hill et al., 1990) and recent relocations by Prejean (2001) indicate magma movement from initial depths of 7-9 km to within approximately 1 km of the mountain's surface over that six month time period.

The following spring (1990), an unusually heavy loss of needles was observed at several places on Mammoth Mt. by U.S. Forest Service personnel (Farrar et al., 1995), especially surrounding the popular recreation area of Horseshoe Lake. Approximately 4 ha of trees were dead at this lake alone, affecting all species of trees and other forest vegetation. Their deaths were initially attributed to the Sierran drought of the 1980's. In 1994 however, soil gas measurements made by the USGS confirmed that the kills were likely due to asphyxiation of the vegetation via the presence of 30-96% CO_2 in the ground around the volcano (Farrar, 1995). Current flux estimates for the entire mountain are approximately 300-500 tons/day, while flux at the Horseshoe Lake tree-kill is 93 $\pm$ 22 tons/day (Rogie, 2001). Background concentrations of CO_2 in this region are approximately 360 ppm, however concentrations in tree-kill zones can be upwards of 10,000-100,000 ppm early in the day (Rogie, pers. comm., March 2000). Many areas of CO_2-induced kills are now identified on Mammoth (Figure 2).

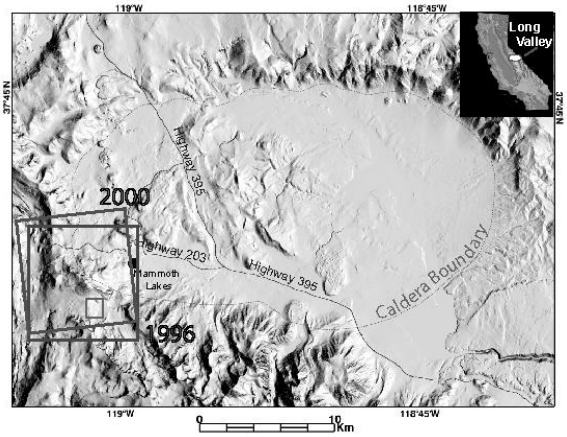

Figure 1. Shaded relief digital elevation model image of Long Valley Caldera. The scene boundaries of both years of AVIRIS data are shown as well as the approximate boundary of aerial photo and HyMap data scenes used.

Traditional mapping of CO_2 discharge zones on Mammoth Mt. is done on-foot with portable accumulation chamber instruments and GPS. The remote sensing techniques described in this study are accomplished remotely, making the spatial and temporal mapping of volcanogenic-assisted forest deaths easier and quick to do. Such mapping is vital for geological, forest, ski, and city personnel in charge of determining areas and level of hazard at Mammoth Mt. Mapping of tree-kill zones with aerial photography and hyperspectral imagery was done previously (Hausback et al., 1998; Sorey et al., 1998; de Jong, 1998; Martini et al., 2000), however this study presents the kills through time. It also attempts to utilize the superior calibration and fine spectral sampling of Advanced Visible/Infrared Imaging Spectrometer (AVIRIS) to identify and map the characteristic spectral absorptions of CO_2 gas within the near-infrared portions of the electromagnetic spectrum (2.00-2.50 μm). The following sections address the genesis of the tree-kills on Mammoth, their growth through time, and initial attempts at detection and mapping of anomalous CO_2 in the atmospheric column above Mammoth Mt. A compilation of aerial photo, HyMap data, and AVIRIS data are used in this endeavor.

[1] University of California Santa Cruz, Earth Science Department, Santa Cruz, California 95064, USA
bmartini@es.ucsc.edu

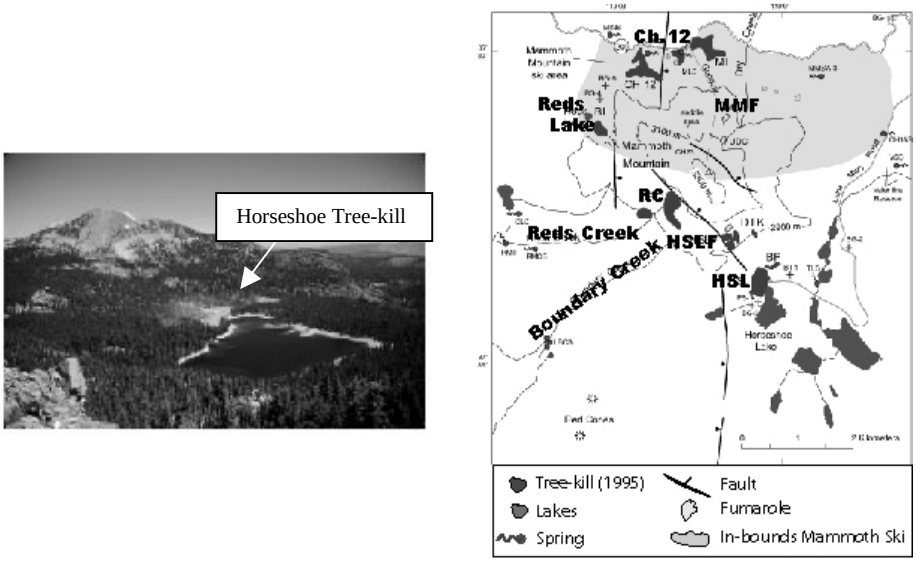

Figure 2. Picture on the left looking northeast with Horseshoe Lake in the forefront and Mammoth rising to the left. The tree-kill is visible on the northern shore of the lake. Map on the right showing known CO_2-induced tree-kills on Mammoth Mt.

2.0 PREVIOUS TREE-KILL BOUNDARY AND CO_2 MAPPING EFFORTS

The tree-kill distributions on Mammoth Mountain were initially mapped using large-scale 1:14,500 aerial photography dating from 1995 (Farrar et al., 1995; Sorey et al., 1998). The boundaries of a few specific kills were also surveyed using handheld GPS receivers, as well as two-color geodimeter measurements. Horseshoe Lake garnered early attention due to the massiveness of the kill and the large measured CO_2 flux: its boundary was measured twice using GPS; once in 1994 (Farrar et al., 1995) and once more in 1998 (Rogie and Colvard, unpub. data, 1998). The above methods are time-intensive and necessarily limited by the subjectivity of human observers on the ground.

Two separate studies in the late 1990's used hyperspectral imaging to assess the boundaries of tree-kills on Mammoth Mountain. The results of both de Jong (1996; 1998) and Hausback et al. (1998) provided initial success at mapping tree mortality using 20 meter resolution AVIRIS data. Hausback et al. also attempted to spectrally discriminate stressors or sources of tree-morbidity on the mountain (eg. the differences between trees killed by CO_2 versus those killed by drought, insects, fire, flooding, etc.). This proved to be less straightforward.

Initial attempts at mapping volcanogenic CO_2 with AVIRIS data was completed on the northern flank of Mammoth Mt. (de Jong and Chrien, 1996). Their results were inconclusive: both CO_2 endmembers acquired in the field and a ratio algorithm targeted at CO_2 band depth at 2.01 μm did not reveal zones of known CO_2 flux in 1994 or 1995 AVIRIS data. There is also ongoing work to quantify CO_2 concentrations in the atmosphere (Green, 2001). Such work has been successful, however detection of small increases or decreases in CO_2 concentration in the atmospheric column (several tens of ppm) appear difficult to track and measure.

3.0 A TEMPORAL ANALYSIS OF HORSESHOE LAKE TREE-KILL GROWTH SINCE 1989

3.1 Timeline of tree-kill growth: unanswered questions

Tree-kills were first noticed in 1991 at several locations around Mammoth Mountain including Horseshoe Lake on the southern flank and Chair 12 and Reds Lake on the northern flank. Several other kills around the mountain appeared in the years following 1991 including Reds Creek on the western flank and several kills on the north face of the mountain inbounds of the resort. Cook et al., 2001 determined through radiocarbon measurements at the Horseshoe Lake kill that almost all the trees sampled there began fixing less carbon-14 beginning in 1990. This deficiency in carbon-14 in 1990 due to magmatic CO_2 uptake was also measured at Reds Creek. The work of Cook et al. indicated that peak flux occurred in 1991, decreased steadily from 1991 to 1995, and was fairly constant till 1998. In addition, measurements of trees near cold CO_2-rich springs on the flanks of Mammoth indicate that

degassing via groundwater has been occurring in at least one tree, since 1967. This is some of the only quantitative knowledge we have about how the tree-kills have grown through the years. However, we still don't know how the tree-kills grew spatially, as none of their boundaries were actually surveyed until 1995. Knowing their initial region of death and the subsequent trajectory of growth of the kill boundaries reveals important information about the subsurface structural system and how the CO_2 propagates. We have attempted to determine a semi-quantitative measure of the growth of the tree-kill at Horseshoe Lake via a multi-temporal airborne remote sensing data analysis. Several techniques are used in this study to accurately identify the boundaries of the tree-kill at Horseshoe Lake over a period stretching from pre-kill times to recent (1977-1999). It elucidates how the kill at Horseshoe Lake began, how it grew, and whether it has continued to expand. The success of this analysis is grounds for its employment at other kills on the mountain.

3.2 Historical air photo analysis

3.2.1 Methods

Air photos of differing scales and seasonal character were acquired and analyzed for the years, 1977, 1990, 1993, 1994, and 1995. A hyperspectral 1999 HyMap image was also used in this analysis. Each photograph was scanned in at 800dpi and saved as a TIFF. The photos were subset to include the Horseshoe Lake tree-kill and 1-2 km of area surrounding the lake. The approximate location of these photos and hyperspectral image is shown by the smallest rectangle over Mammoth Mt. in Figure 1.

Several different methods were used to determine the boundaries of the kills in each photo. Simple enhancement techniques such as linear and gaussian stretching were used for delineating kill boundaries. All of the color photos were actually color-infrared, and hence dead or dying vegetation appeared less red and thus less healthy in near-infrared photography. Stretching of the data values contained in each photo allowed for simple tree-kill boundary identification and mapping. More sophisticated methods such as the Minimum Noise Fraction (MNF) algorithm contained in ENVI© were also applied to the photos. The black and white photo from 1993 was a bit more difficult. The tree-kill is visible in this photo, but doesn't stand out as well as it would in the color-infrared photography. Simple stretching didn't work well with this photo and the single panchromatic band precludes MNF analysis impossible. All the boundaries are hand-digitized into regions of interest (ROIs) and exported to separate vectors. The area of each vector polygon was calculated in hectares and is reported in the inset table of Figure 3.

Each photo was then georectified using 30-50 ground control points. RMS errors were generally below 1 to just around 2, but never went above 5. This translates to approximately 2-3 pixels (40-60 m) of errror. Visual comparison of georectified photos with each other was very good.

3.2.2 Results

The MNF mapped the tree-kills well, however the simple stretching techniques were equally successful. Considering the time, storage space and effort required for an MNF, we submit that stretching routines are adequate. Figure 3 shows the vectors from all five years including the vector from the 1999 HyMap data derived from unmixing methods within ENVI©. Horseshoe Lake is placed at the bottom for reference. Minor discrepancies in boundaries are likely due to georectification error and boundary delineation error. The boundary delineation for the panchromatic 1993 photo was least successful. We erred towards the conservative with this year and hence the boundary contains less detail. Excursions in the 1999 HyMap data are due to the increased measurability of tree morbidity and sub-morbidity (the so-called "halo zones" of the tree-kill). However major boundary excursions, such as that seen between 1993 and 1994, are likely real and not due to analysis error. A plot of the growth of the tree-kill through time is shown as an inset of Figure 3.

3.3 The growth of the Horseshoe Lake Treekill: new temporal and spatial patterns revealed

The tree-kill as of 1990 was approximately 4.1 Ha including the beginnings of the northern Borrow Pit kill which was previously thought to have appeared later in 1993 (Cook et al., 2001). From 1990 to 1993, the main kill didn't change much in size. However, the Borrow Pit kill continued to grow, and a new satellite kill appeared to the south of the main kill. From 1993 to 1994, the tree-kill at Horseshoe Lake grew from approximately 5.2 Ha to 10.9 Ha, almost doubling in size. This is a previously unrecognized event. Cook et al.'s work doesn't indicate an increase in degassing in this time period. However, we may be seeing the delayed effects of the initial pulse of CO_2 degassing at Horseshoe Lake. Cook et al. indicates that trees towards the center of the kill experienced the CO_2 pulse first and hence died fastest. This is supported by the present analysis that shows initial kill in 1990 towards the center of the current kill zone (see Figure 3). Trees lying directly in ground zero of the CO_2 flux zone were

killed immediately. Transpiration and mineral and water uptake would have ceased. Initially high airborne CO_2 levels seen in the kill during this initial time period (1200 tons/day (Farrar et al., 1995)) probably led to widening of the stomata in the conifer needles to accept more CO_2 (which plants normally like) (Larcher, 1995). However, to ward off increasingly noxious levels of CO_2, plant stomata probably closed completely. The trees quickly ceased respiration and photosynthesis. They were effectively suffocated. Their cells ceased to function and the trees died.

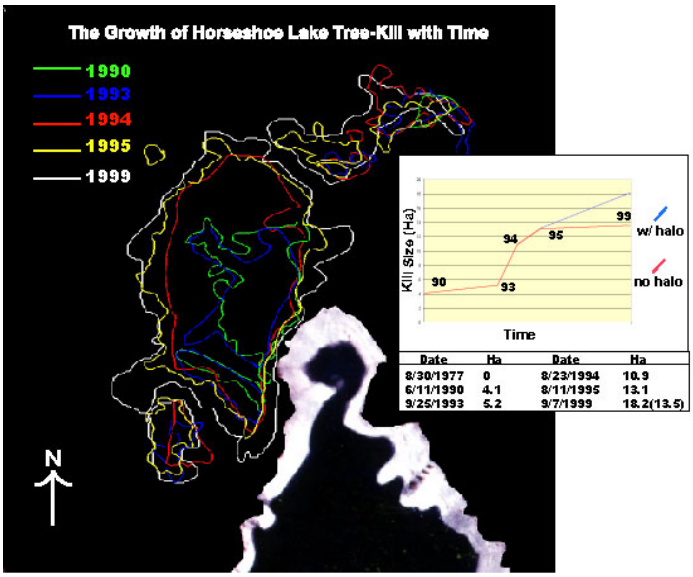

Figure 3. Tree-kill boundaries through time at Horseshoe Lake. Boundaries determined through analysis of both historical aerial photography and hyperspectral data. Inset plot shows the growth of the kill in ha.

Trees towards the boundaries of the kill away from the main CO_2 source zone, might not have received such a strong initial pulse. The CO_2 received did cause initial stress on the physiological systems of the trees. Chronic flux continued to weaken these more peripheral trees until many of them finally died after the particularly hard winter of 1993-1994. It is well known that a combination of stressors on an ecosystem is more lethal than merely one stressor and hence the heavy snows and late spring served to exacerbate the CO_2 stress problem. In addition, Cook et al. found that peripheral trees tended to die approximately four years after initial deficiencies in carbon-14 were measured. The above scenario may explain why the tree-kill is not rapidly growing at present. Constant flux from an anchored point source keeps border trees in a state of heightened physiological stress. Other stressors such as drought or insect infestation may lead to new kills, but current kills will probably remain constant in size. Future kill zones may not be due to anomalous CO_2 flux and thus possible future kill sites should be surveyed for other external stressors such as insects or drought.

The above set of analyses could easily be done for other kill sites on Mammoth Mt. As previously mentioned, Cook et al.'s radiogenic measurements on trees from Reds Creek indicated CO_2 flux in this region at least since 1967. Multi-temporal air photo analysis could reveal when trees began to die at Reds Creek historically, as well as when trees began to die around the Mammoth Mt. after the 1989 seismicity. Any correlation between timing of individual kills may indicate similar shared gas sources at depth and shared, networked, subsurface connections (such as faults and fractures). In fact, the current pattern of kills appears to coincide with hypothesized ring fractures on Mammoth Mt. (Prejean, 2001).

4.0 DETECTING AND MAPPING VOLCANOGENIC CO_2 IN THE ATMOSPHERIC COLUMN ABOVE MAMMOTH MT.

4.1 Spectroscopy of CO_2

Gas absorptions form primarily in response to vibrational absorption processes. For CO_2, there are nine fundamentals (vibrational modes). The stretching and bending of the bonds in the internal modes produces the infrared absorptions seen in CO_2 spectra. In addition, when CO_2 makes a vibrational transition, it usually makes a rotational one as well. CO_2 thence has three vibration-rotation bands (two of which are the same frequency) and a fourth band that is infrared inactive. Other absorptions are seen in CO_2 spectra, and these are due to overtones and combinations of the original fundamentals. The near-infrared absorptions of interest in this study are combination bands centered around 2.0 μm. They have centers at 1.96 μm, 2.01 μm and 2.06 μm. Each absorption is actually a doublet. The main absorption feature of interest used in this study is the 2.06 μm band whose doublet lays longward at 2.08 μm (see Figure 4). Intensity of absorptions are affected by both the level of fundamental mode (fundamentals have higher intensities of absorption than overtones and combinations do) (Gaffey et al., 1993), and the relative amount of the material causing the absorptions (the total absorptance increases with the amount of

material present)(Schurin and Ellis, 1968). Widths of bands are greatly affected by temperature and pressure, with increasing values causing absorptions to widen.

4.2 AVIRIS analysis: spectral detection of anomalous CO_2

The analysis goal was to determine whether anomalous levels of CO_2 are detectable in the atmospheric column using AVIRIS radiance data. Two separate years of data were utilized in this study; 1996 and 2000. Scene boundaries were chosen to encompass the massif of Mammoth Mt. as well as some outlying regions known to be volcanically active in the recent geologic past. Boundaries for both the 1996 and 2000 scenes are shown in Figure 1.

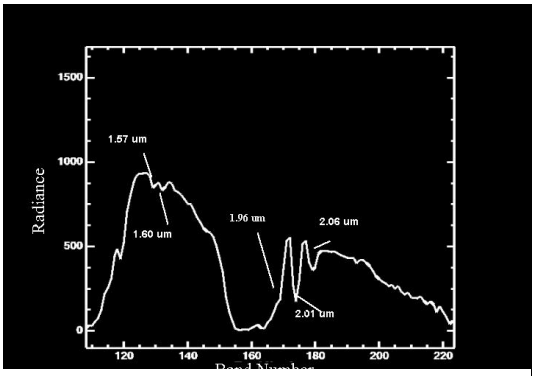

Figure 4. Spectral signature showing major CO_2 absorption regions

Both years of data were subjected to the same analysis methodologies. The data were spatially subset, spectrally subset, and analyzed for unique, repeatable, spectral features in the 2.0 μm CO_2 absorption wavelength region. In the wavelengths measured by AVIRIS, there are three CO_2 absorption regions: 1.4 μm, 1.6 μm, and 2.0 μm. This study was limited to analysis of the absorptions centered around 2.0 μm as the 1.4 μm absorptions lie too close to the H_2O absorption maximum at 1.38 μm, and the shallow 1.6 μm absorptions were not discriminated from background noise. Though the 2.01 μm feature has the highest absorption intensity, we chose the 2.06 μm absorption feature (seven bands spanning 2.04-2.10 μm). We found it to be less vulnerable to contamination from the wings of the strong 1.87 μm H_2O band. All major and minor water bodies were masked before any spectral analysis. This was done both to reduce the spectral variability encountered in the scene and to reduce the effects of the 1.87 μm water band on the 2.06 μm CO_2 absorption

Continuum Removal (CR) and Minimum Noise Fraction (MNF) processing were applied to both years of AVIRIS data. We theorize that anomalous levels of CO_2 degassing from Mammoth Mt. will be detectable above background levels. Band depths in regions of elevated flux will be higher than expected given a certain elevation. Those regions with deeper than expected absorptions are possible point sources of magmatic CO_2 degassing. Normal CO_2 at these elevations is approximately 360 ppm, which is approximately 0.04% of the gasses in the atmospheric column measured by AVIRIS. Minor concentration variations from 360 ppm are difficult to measure (Green, 2002). However CO_2 concentrations at several locations on Mammoth Mt. reach levels of 10,000 – 100,000 ppm. It may be possible to detect CO_2 concentrations approaching 10 % in the atmospheric column.

4.2.1 AVIRIS analysis: Continuum Removal

CR was performed on the 2.06 μm absorption feature region in both years of AVIRIS radiance data. Theoretically, the more CO_2 there is in the atmospheric column, the deeper this absorption feature will be. Since there is a direct correlation between the amount of a gas and the relative depth of its absorption, a CR applied to the data should reveal those regions in an image dataset with higher amounts of CO_2 in the atmospheric column. Deeper absorptions should relate to increased levels of CO_2, while more shallow absorptions should relate to decreasing levels of CO_2. Differing depths of absorption were delineated with an arbitrary density slice of the final CR image.

4.2.2 AVIRIS analysis: Minimum Noise Fraction

The second analysis performed on the data was the MNF. The MNF is basically two cascaded principle component transformations, where the first transformation decorrelates and rescales the noise such that the noise has unit variance and no band-to-band correlations, and the second transform takes the noise whitened data and puts it through a standard Principle Components calculation. The MNF transformed data were analyzed on an image-by-image basis where each coherent image may emphasize a particular class of material. By focusing in on a particular absorption (2.06 μm), it was hoped the material causing said absorption would be represented in one of the coherent MNF images.

4.2.3 AVIRIS analysis: Results

Figure 5 shows the results of the CR with an eight level density slice applied. The deepest absorptions are shown in red. The next deepest are shown in green, then blue, yellow, cyan, magenta, maroon, and seagreen respectively. An elevation effect should be discernable in the data: higher elevations should have less overall CO_2 and a shallow CO_2 absorption feature while lower elevations should provide a much deeper absorption feature due to the increased amount of CO_2 in the atmospheric column (Green, 2001). Mammoth Mt. located in the lower southeast corner of the image rises approximately 600 m above the surrounding landscape. As such, higher elevations of the mountain are colored in green, blue, yellow, etc. while surrounding terrain is colored red. The blue coloration on the summit of the mountain indicates a more shallow absorption than the red coloration on its flanks, which indicates a deeper absorption. The CR algorithm appears to work at this regional scale, however regions known to host anomalously high CO_2 flux levels are not identifiable on this CR image. Average spectral signatures extracted from each density class show an expected pattern of deeper absorptions for lower elevations and more shallow absorptions for higher elevations (see Figure 5). Also of note, though the main absorption is located at 2.06 μm, CR analysis has brought out an absorption centered at 2.08 μm. Its depth appears to be conversely related to elevation, i.e. the higher elevations have a deeper 2.08 μm absorption than the lower elevations. This is opposite to the absorption depth/elevation relationship for 2.06 μm.

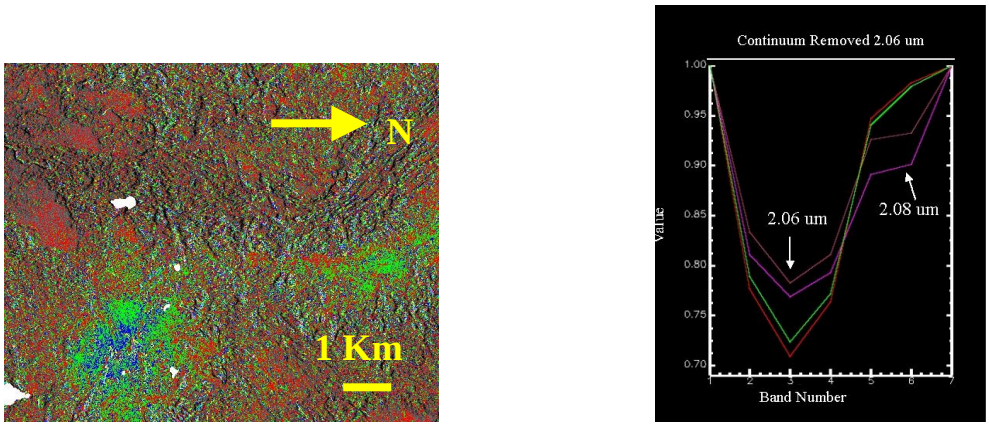

Figure 5. Subset of 2000 AVIRIS image shown on the left. A continuum removal has been applied to the 2.06 μm CO_2 absorption feature from 2.04 – 2.10 μm. The resulting image was density sliced into eight arbitrary color levels. The spectra on the right are average signatures extracted from selected density classes.

The results from the MNF analysis are more compelling than that achieved with the CR, however they are more complex. Four of the seven bands analyzed in the 2000 imagery were coherent, while only three of the seven bands were coherent in the 1996 imagery. In the 2000 AVIRIS image, MNF band 3 appears to contain a spatial distribution of degassing CO_2, while in the 1996 AVIRIS image, it's MNF band 2 that reveals a CO_2 distribution similar to that known to exist from previous field studies (Sorey et al., 1998; Rogie et al., 2001). Figure 6 shows results from the MNF analysis of 2000 AVIRIS imagery. A density slice was applied to MNF band 3. The most extreme values of the MNF (i.e. the highest density slice) were then isolated and highlighted. These areas are plotted on top of the georectified MNF band 3 image along-side mapped faults of the region.

Results from the MNF analysis on 1996 AVIRIS imagery produced similar distributions as those seen in the 2000 imagery. There are some high MNF value zones not seen in the 2000 imagery, as well as zones identified in the 1996 image that do not appear in the 2000 image. Figure 7 shows both years of extreme MNF-value zones. The zones appear around the mountain, occurring on varying rock types, differing elevations, and in both tree-covered and tree-less landscapes.

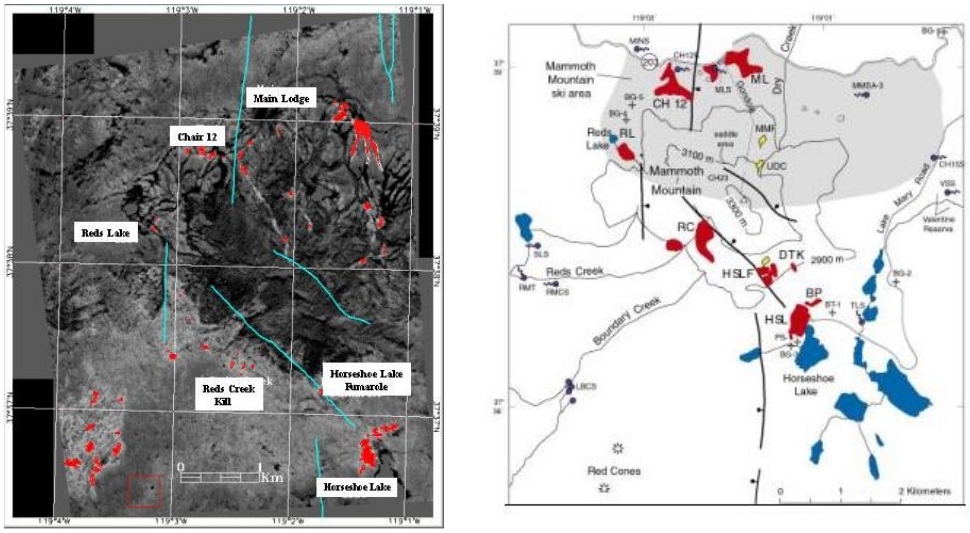

Figure 6. Results from the MNF transformation of 2000 AVIRIS imagery. MNF band 3 is shown with a density slice derived map of extreme MNF values in red. A map of known tree-kills in red is shown on the right (note different scale).

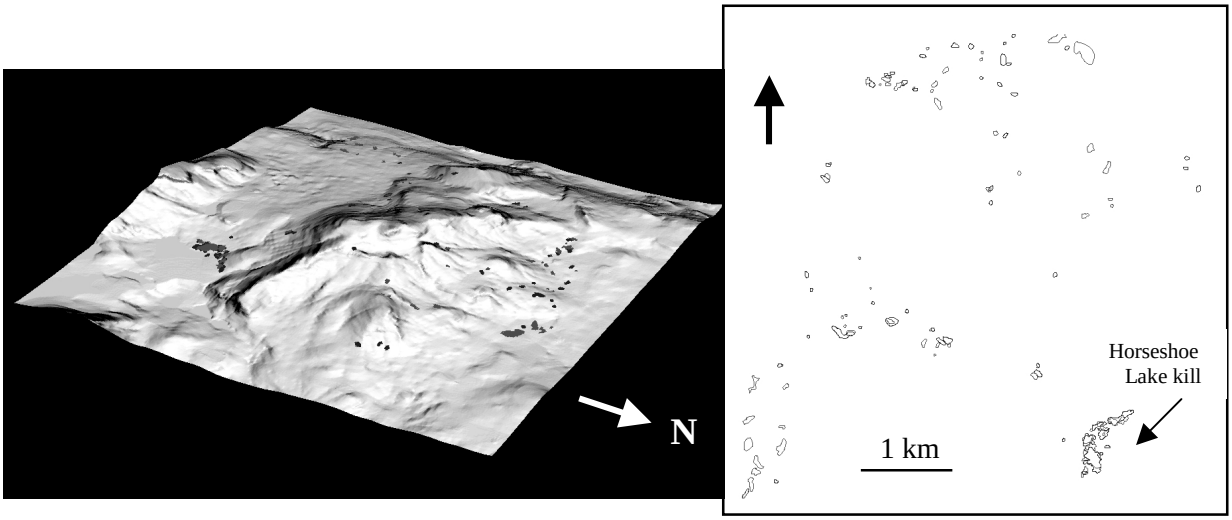

Figure 7. Left: results of MNF analysis of the 2.06 µm CO_2 absorption for 1996 (darker) and 2000 (lighter) AVIRIS imagery. Extreme MNF values from MNF band 2 (1996) and MNF band 3 (2000) shown draped on a shaded 10m USGS DEM. Right: Both years of extreme MNF values shown in plan view.

4.3 Discussion: Feasibility and problems with anomalous CO_2 detection and mapping

The general success of the CR analysis in mapping gross amounts of CO_2 in the atmospheric column is encouraging. However, the inability to map regions of extremely high concentrations of CO_2 at several major tree-kill sites with a simple CR analysis was disappointing. One problem may be that the CR/density slice analysis only measures the depth of the 2.06 µm absorption at its maximum minima. The prominence of the 2.08 µm absorption longward of the main 2.06 µm absorption may hold the key to part of the problem. This 2.08 µm absorption is probably the second half of the 2.06 µm doublet. The fact that it appears to be sensitive to elevation in a converse way to the 2.06 µm absorption is undoubtedly important. A CR analysis of just this absorption (3 bands centered on 2.08 µm) may reveal a more compelling CO_2 flux zone pattern. Another way to investigate the 2.06 µm absorption may be an area-of-absorption analysis. The calculation of band depth normalized to absorption feature areas is found to closely follow amounts of plant biochemical constituents such as water, chlorophyll, cellulose, sugar, etc.

(Kokaly and Clarke, 1999; Curran et al., 2001). Perhaps similar area calculations would prove viable for CO_2 gas absorptions.

The MNF results are quite compelling, though poorly constrained. We cannot know exactly what the MNF is detecting. It is mapping levels of coherence, but the classes produced from this procedure do not possess unique spectral signatures like other endmember classes we are used to. We initially assumed that extreme values of MNF band 3 (2000 data) were detecting anomalous levels of CO_2 via a deeper 2.06 μm absorption relative to surrounding pixels containing more shallow absorptions in this wavelength region. We theorized that these deepest absorptions were different enough from neighboring pixel values, that they produced their own MNF coherence band. The resulting spatial distributions of the extreme MNF values for both 1996 and 2000 are almost perfect matches to known zones of volcanogenic CO_2 flux, some of which host tree-kill sites. However, there are a few exceptions, which may hold the key to determining what the MNF transform analysis is actually detecting.

There are two major sites in the 2000 image mapped as extreme in MNF band 3 that do not correspond to any known zones of CO_2 flux or CO_2-induced tree-kill sites. These include zones mapped in the Rainbow Fire kill of 1992 and zones mapped at Chair 2 on the northern flank of Mammoth in-bounds of the ski area. Groundtruthing with a portable gas accumulation chamber in July, 2002 at these two sites revealed no anomalous CO_2 flux. However, both sites contained an excess of cellulose and lignin in the form of dead trees (at the Rainbow Fire site) and dry mulching grass (spread over the ski-runs at Chair 2 to increase slope stability). The grass possesses a good deal of cellulose, while the dead trees contain both cellulose and lignin within the bark and wood. The biochemicals cellulose and lignin have several distinctive absorptions, one of which is centered on 2.10 μm (see Figure 8A). The 2.06 μm CO_2 absorption lies on the shortward wing of these broad biochemical absorptions (see Figure 8B). If you only look at straight reflectance data, the lignin/cellulose absorption doesn't appear capable of greatly affecting spectral analysis. However, analysis of the data included spectrally subsetting the image to only seven bands around the absorption, and CR processing. If we apply the same analysis steps to the spectra of lignin and cellulose, prominent absorptions are revealed at 2.06 μm (see Figure 8C).

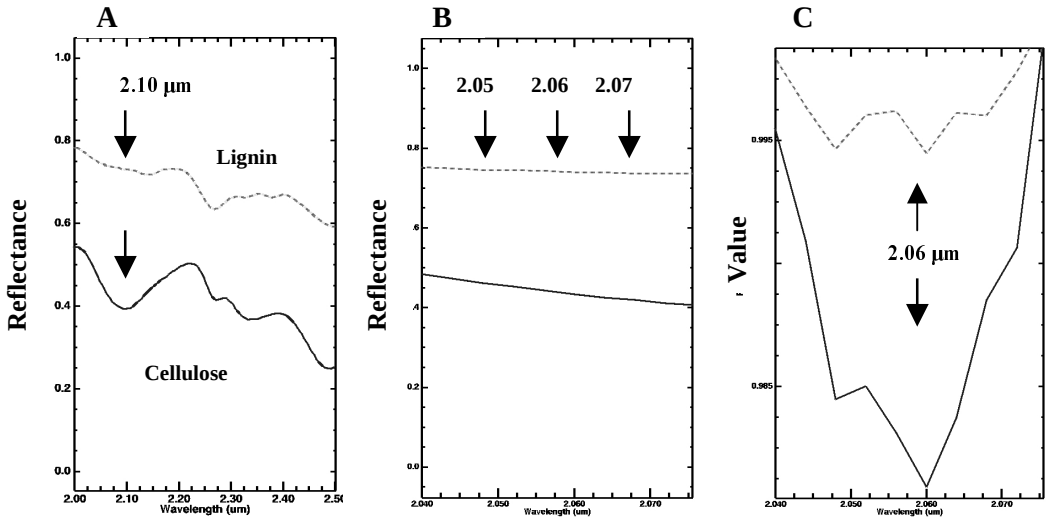

Figure 8. A: Spectral signatures of the plant biochemicals, lignin and cellulose, extracted from the USGS vegetation library B: A close up of these plant chemicals centered around 2.06 μm C: Continuum removed spectral signatures of the same chemicals shown in 8B.

This suggests that the presence of excessive dead trees and grass may create a landscape that would be preferentially mapped when using a density sliced, directed MNF transform of the 2.06 μm absorption. Most CO_2 flux zones on Mammoth have an abundance of dead or dying trees accompanying them. Perhaps the MNF analysis described in this paper is merely mapping cellulose/lignin in the form of dead trees associated with volcanogenic CO_2 emission zones. However, there is one problem with this scenario. There are a myriad of other dead tree areas on and around Mammoth measured by AVIRIS that are not highlighted with the directed MNF analysis of the 2.06 μm absorption. These include large areas of trees killed by avalanche, flooding, snow and trash burial, and insect infestations. This result suggests that there is something unique about the dead tree cellulose/lignin absorptions

highlighted with the MNF analysis in this paper. Perhaps the MNF analysis is capturing both sources of absorption, i.e. the cellulose/lignin absorption from the dead trees and grass is adding into the anomalous CO_2 absorption. We currently can't constrain how much of each spectral endmember is adding into the final spectral signature. What is unequivocal, is the creation of a map of volcanogenic CO_2 flux zones far surpassing those previously created, in detail and completeness, using standard surveying techniques.

5.0 CONCLUSIONS

Multi-temporal air photo analysis has revealed new spatial and temporal patterns of the CO_2-induced Horseshoe Lake tree-kill. The success of this analysis at Horseshoe indicates that similar analyses on other parts of Mammoth, would be an efficient way of determining the temporal growth of the kills as a whole. Our attempts at detecting and mapping anomalous volcanogenic CO_2 in the atmospheric column produced compelling spatial distributions of CO_2 flux zones that matched quite well with known, previously mapped flux zones. However, this analysis is ultimately complicated by an unknown relationship between CO_2 absorptions and those absorptions from plant biochemicals. Further work aimed at quantifying this relationship should be undertaken.

6.0 REFERENCES

Cook, A.C., L.J. Hainsworth, M.L. Sorey, W.C. Evans, J.R. Southon, 2001, "Radiocarbon studies of plant leaves and tree rings from Mammoth Mountain, CA: a long-term record of magmatic CO_2 release," Chem. Geo., v.177, pp. 117-131.

Curran, P.J., J.L. Dungan, D.L. Peterson, 2001, "Estimating the foliar biochemical concentration of leaves with reflectance spectrometry: Testing the Kokaly and Clark methodologies," Rem. Sens. Env., v.76, pp. 349-359.

De Jong, S.M. and T.G. Chrien, 1996, "Mapping volcanic gas emissions in the Mammoth Mountain area using AVIRIS," Summaries of the Sixth JPL Airborne Earth Science Workshop, March 4-8, pp. 75-81.

De Jong, S.M., 1998, "Imaging spectrometry for monitoring tree damage caused by volcanic activity in the Long Valley caldera, California," ITC Jour., 1998-1, pp. 1-10.

Farrar, C. D., M. S. Sorey, W.C. Evans, J.F. Howle, B.D. Kerr, B. M. Kennedy, C.-Y. King, and J.R. Southon, 1995, "Forest-killing diffuse CO_2 emission at Mammoth Mountain as a sign of magmatic unrest," Nature, v. 376, pp. 675-677.

Gaffey, S. J., L.A. McFadden, D. Nash, C. M. Pieters, 1993, "Ultraviolet, visible, and near-infrared reflectance spectroscopy: laboratory spectra of geologic materials," in Remote Geochemical Analysis: Elemental and Mineralogical Composition, C. M. Pieter and P.A. Englert editors, Cambridge Univ. Press, Cambridge, pp. 43-71.

Green, R. O., 2001, "Measuring the spectral expression of carbon dioxide in the solar reflected spectrum with AVIRIS," Summaries of the Tenth JPL Airborne Earth Science Workshop, February 6-9, pp. 181-192.

Hausback, B. P., M. Strong, C. Farrar, D. Pieri, D., 1998, "Monitoring of volcanogenic CO_2-induced tree kills with AVIRIS image data at Mammoth Mountain, California," in Summaries of the Seventh Annual JPL Airborne Earth Science Workshop, January 12-15.

Hill, D.P., W.L. Ellsworth, M.J.S. Johnston, J.O. Langbein, D.H. Oppenheimer, A.M. Pitt, P.A. Reasenberg, M.L. Sorey, S.R. McNutt, 1990, "The 1989 earthquake swarm beneath Mammoth Mountain, California: an initial look at the 4 May through 30 September activity," Bull. Seis. Soc. Am., v. 80, n. 2, pp. 325-339.

Kokaly, R.F. and R.N. Clark, 1999, "Spectroscopic determination of leaf biochemistry using band-depth analysis of absorption features and stepwise multiple linear regression," Rem. Sens. Env., v.67, pp. 267-287.

Larcher, W., 1995, Physiological plant ecology. 3rd ed., Springer, Berlin.

Martini, B. A., E.A. Silver, D.C. Potts, W.L. Pickles, 2000, “Geological and geobotanical studies of Long Valley Caldera, CA, USA utilizing new 5m hyperspectral imagery,” in Proceedings of the Thirteenth IEEE International Geoscience and Remote Sensing Symposium, Honolulu, HI, July 2000.

Prejean, S.G., 2001, The interaction of tectonic and magmatic processes in the Long Valley Caldera, California, PhD Dissertation, Stanford.

Rogie, J. D., D.M. Kerrick, M.L. Sorey, G. Chiodini, D.L. Galloway, 2001, “Dynamics of carbon dioxide emission at Mammoth Mountain, California,” Earth and Planetary Sci. Lett., v.188, pp. 535-541.

Schurin, B. D. and R.E. Ellis, 1968, “Integrated intensity measurements of carbon dioxide in the 2.0-u, 1.6-u, and 1.43-u regions,” Applied Optics, v. 7, n. 3, pp. 467-470.

Sorey, M. L., W.C. Evans, B.M. Kennedy, C.D. Farrar, L.J. Hainsworth, B. Hausback, 1998, “Carbon dioxide and helium emissions from a reservoir of magmatic gas beneath Mammoth Mountain, California,” J. of Geophys. Res., v.103, n. B7, pp. 15,303-15,323.